



# IRAM Memo 2017-1

## Observational examples of spectral line calibration at the 30m telescope with **MRTCAL** and **MIRA**

C. Marka<sup>1</sup>, J. Pety<sup>2,3</sup>, S. Bardeau<sup>2</sup>, A. Sievers<sup>1</sup>

1. IRAM (Granada)
2. IRAM (Grenoble)
3. Observatoire de Paris

Sep., 14<sup>th</sup> 2017  
Version 1.0

### Abstract

Since February 2017, **MRTCAL** has replaced **MIRA** as the software for spectral line data calibration (except polarimetry and continuum) at the 30m-Telescope. Slight changes in the calibrated spectra are expected, for example in form of an improved calibration accuracy at the edges of the atmospheric windows as result of the narrower calibration bandwidth used by **MRTCAL** (20 MHz by default, compared to up to about 1.35 GHz for **MIRA**). This report demonstrates the practical performances of **MRTCAL** by a systematic comparison of observations calibrated with both softwares.

Keywords: **MRTCAL**, **MIRA**, 30m calibration

Related documents: **MRTCAL** documentation, **MIRA** documentation, **CLASS** documentation.

## Contents

1	Qualitative impact of the MRTCAL frequency dependent calibration	3
2	Observations dedicated to the comparison between MRTCAL and MIRA	6
3	Qualitative comparison of raw spectra	6
4	Quantitative comparison of line intensities	7
5	Quantitative impact of the MRTCAL frequency dependent calibration	9
6	Comparison of switching modes	11
7	Calibration stability with time and elevation	12
8	Acknowledgments	12
9	References	12
A	List of used lines	14

# 1 Qualitative impact of the MRTCAL frequency dependent calibration

Differences between **MIRA**- and **MRTCAL**-calibrated spectra are expected as a consequence of the different calibration bandwidths. One value of the calibration parameters are derived and applied per 1.35 GHz natural hardware unit when **MIRA** calibrates FTS200 spectra. In contrast, **MRTCAL** derives and applies the calibration in steps of 20 MHz (in the current default settings for the automatic online data processing; this value can be customized by the user).

The **MRTCAL** default is intended to improve the quality of the baseline, as can be seen on Fig. 1 to 4. The average spectra computed from the same 15 minutes On-The-fly scan is displayed in each of the four figures. The only difference between the four spectra are the way **MRTCAL** calibrates the raw data.

1. In Fig. 1, the calibration parameters are derived and applied per natural hardware unit (*i.e.*, every 1.35 GHz as defined by the FTS units). This gives a staircase look to the spectra.
2. In Fig. 2, the calibration parameters are derived every 1.35 GHz. But they are linearly interpolated before being applied. The staircase look is greatly decreased.
3. In Fig. 3, the calibration parameters are derived and applied every 20 MHz. No linear interpolation is done before application. The staircase look and the baseline oscillations disappeared. The atmospheric line around 110.8 GHz now appears in absorption as it should because the reference position was localized about 1 degree away from the OTF observations.
4. Finally, in Fig. 4, the calibration parameters are derived every 20 MHz and linearly interpolated before being applied. The improvement with respect to the previous solution exists even though it is not obvious on this plot.

**MRTCAL** proposes by default the fourth solution. It thus delivers better behaved baselines. The **MRTCAL** default is also intended to improve the line calibration accuracy in regions where calibration parameters vary quickly as a function of frequency, as shown in Sect. 5.

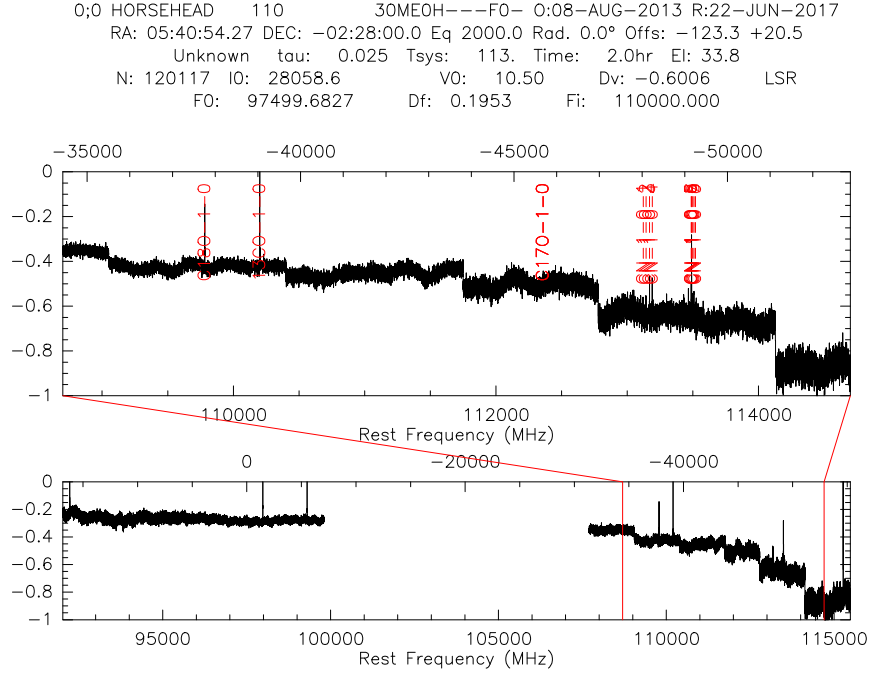


Figure 1: Spectra averaged over a 15 minute On-The-Fly scan observed with a combination of E090 and FTS200 under average summer weather ( $\sim 7$  mm of precipitable water vapor). The simultaneously observed LSB and USB spectra are shown on the bottom panel and a 5 GHz window near the 3 mm band edge is zoomed on the top panel. The calibration parameters are here derived and applied by **MRTCAL** per natural hardware unit (1.35 GHz bandwidth for each FTS unit, i.e., same as MIRA calibration scheme).

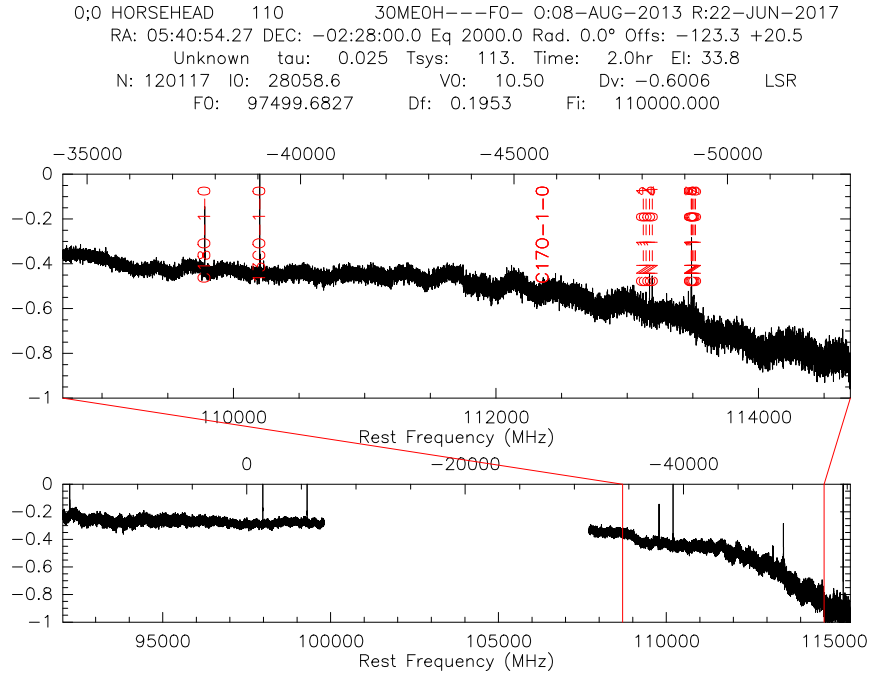


Figure 2: Same as Fig. 1 except that the calibration parameters are now linearly interpolated by being applied.

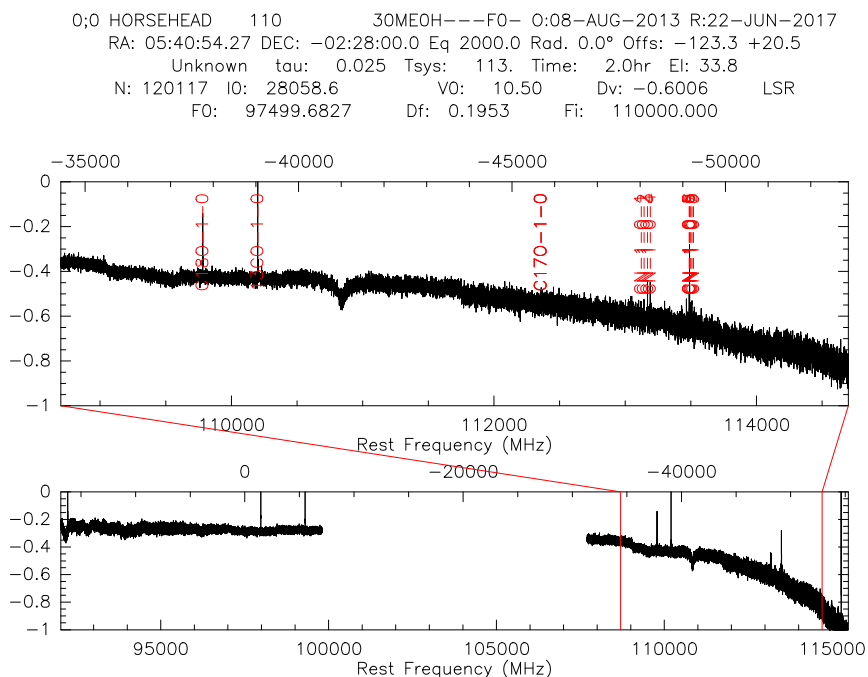
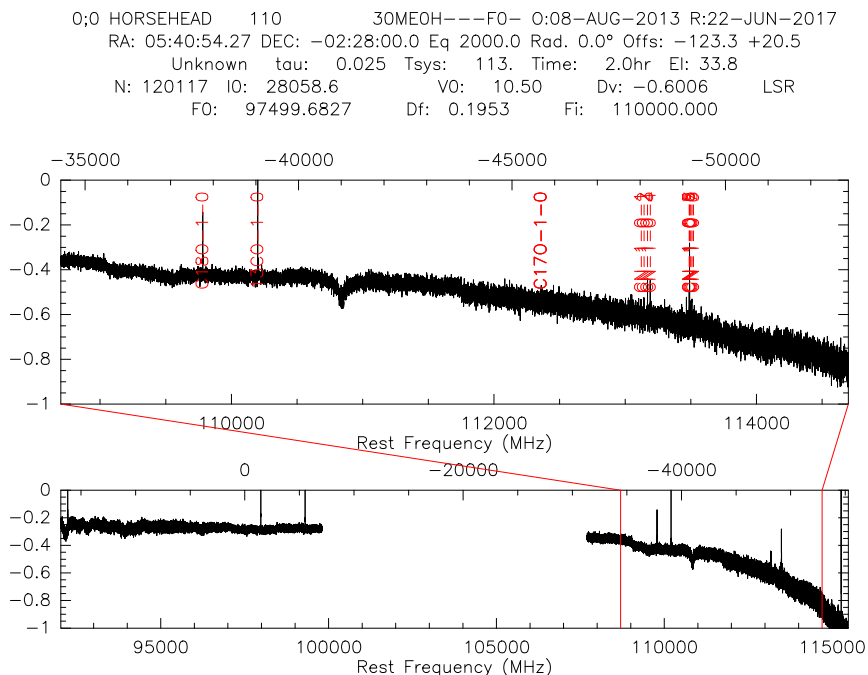


Table 1: Observing setups. The covered frequency range is indicated for FTS200, and the center frequency of the 120 MHz wide windows for VESPA. The last column lists the observing modes for the according setup (with WSW wobbler switching, FSW frequency switching, and PSW position switching).

Tuning	Setup name	FTS200 coverage [GHz]	VESPA center [GHz]	Observing mode
E150 150.000 UI	POINT2MM	147.70–155.48		WSW
E150 176.500 UI	L170250	158.52–166.30 & 174.20–181.98	176.553	WSW
E230 230.500 UI	L224250	212.52–220.30 & 228.20–235.98	217.9102 & 230.538	WSW, PSW, FSW
E330 345.139 UI	L338890	342.84–350.62	345.94	WSW



Figure 5: Two examples of unprocessed VESPA spectra calibrated with **MIRA** and **MRTCAL** (black and red in the lower panels). The upper panels show the difference spectrum. Both polarizations and all consistent scans (same setup and observing mode) have been averaged. The three central channels of each spectrum have been masked as spikes are expected in the center of the three adjacent 40 MHz units for VESPA due to technical reasons (Paubert 2002).

## 2 Observations dedicated to the comparison between MRTCAL and MIRA

Observations on the approximately point-like source IRC+10216 were obtained under the technical time T06-16 during 2016 November 15–17 under mostly stable weather with opacities of 0.1–0.2 at 225 GHz. Four EMIR frequency setups (and one setup for HERA not included in this report) were tested, including the 1mm band around the CO(2–1) line of frequent interest for observers, as well as a setup close to the edge of the atmospheric window of the 2mm band, which is expected to be especially sensitive to the calibration. All spectral line backends - WILMA, FTS in its wide resolution mode, and VESPA configured to 40 kHz resolution and 120 MHz bandwidth - were connected. The 1mm band setup was observed in all three switching modes available for spectral line observations: wobbler switching (designated WSW in the following) observations used a throw of  $\pm 90''$  in azimuth with a phase time of 2 s, frequency switching (FSW) a throw of  $\pm 23.4$  MHz at a phase time of 0.2 s, and position switching (PSW) was done relative to an off position  $600''$  west (in right ascension) of the source. Table 1 lists the observing setups and table 2 lists the spectral lines that are used in the following work.

## 3 Qualitative comparison of raw spectra

Figure 5 compares two **MIRA** and **MRTCAL**-calibrated lines covered at high resolution with VESPA. Figure 6 compares **MIRA** and **MRTCAL**-calibrated FTS spectra for all four frequency setups. In all

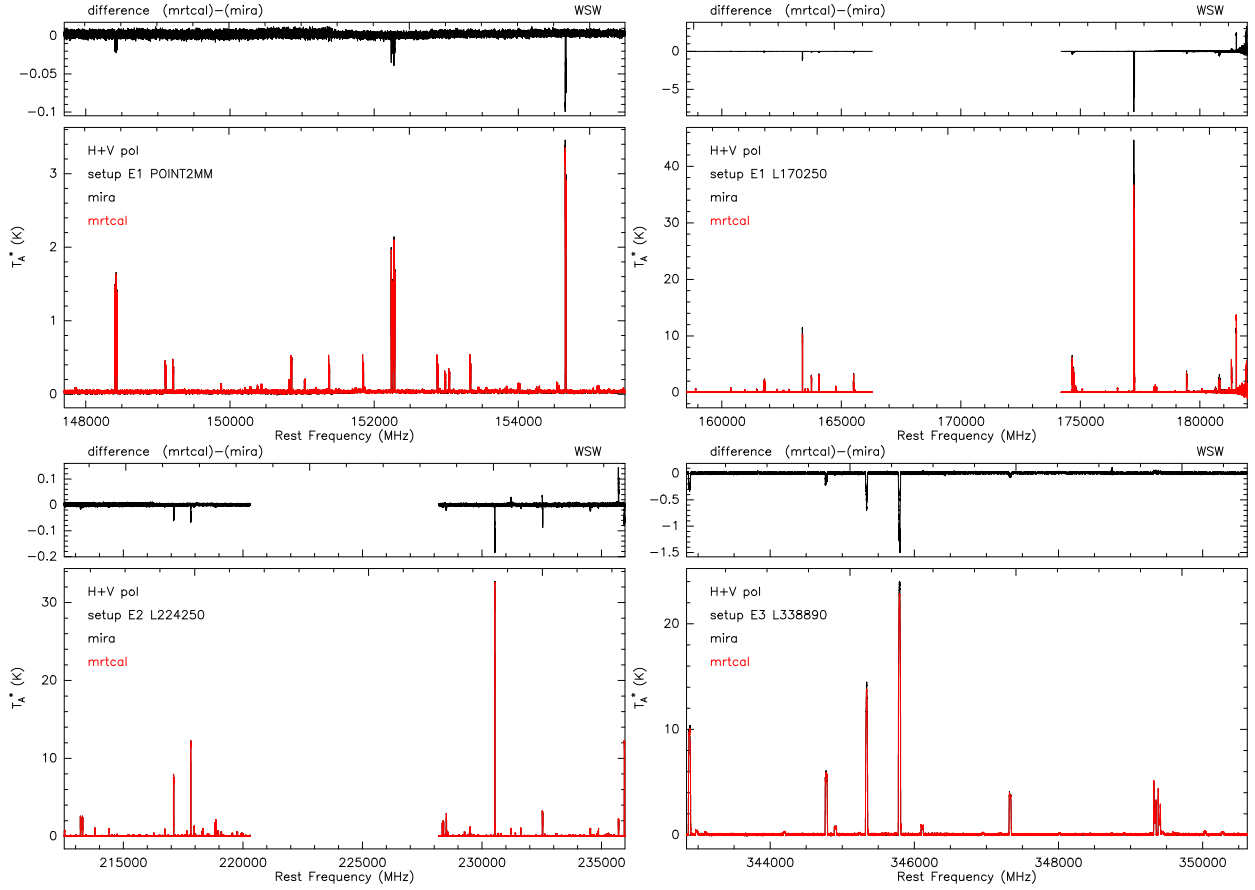


Figure 6: Comparison of unprocessed (except for blanking of spikes and a spurious feature in E3) FTS200 spectra calibrated with **MIRA** and **MRTCAL**. The spectra are overplotted in black and red in the lower panels. The difference spectrum is displayed in the upper panels. Both polarizations and all scans (4 scans for setup E1 POINT2MM and E3 L338890, 6 for E1 L170250 and 10 for E230 L224250) have been averaged for each setup and observing mode, indicated in the upper right of each plot. All visible narrow features are spectral lines.

cases, default calibration settings were used. Both polarizations and all consistent scans were averaged. Spikes and a spurious signal at intermediate frequencies  $5.62$  and  $11.24 \pm 0.01$  GHz in the E330 setup, which stems from interference with a network switch in the backend room, have been blanked. No further processing was applied. In particular, no baselines were subtracted.

The line shape observed at high spectral resolution show variations of the order of at most a few percents (cf. Fig. 5). Systematic differences are discernable on spectral lines in Fig. 6, with either **MIRA**- or **MRTCAL**-calibrated spectra showing higher intensities depending on the frequency. For instance, the differences are exacerbated for setup E150/L170250 that is situated close to the upper edge of the atmospheric window of the 2mm band (it shows a notable increased in the baseline noise at the high frequency end). These differences will be quantified and explained in the next sections

## 4 Quantitative comparison of line intensities

We selected all the lines present in the FTS200 spectra with a signal-to-noise-ratio larger than four. We discarded blended lines, lines from the image side band and “ghost” lines in the E230 setup arising from

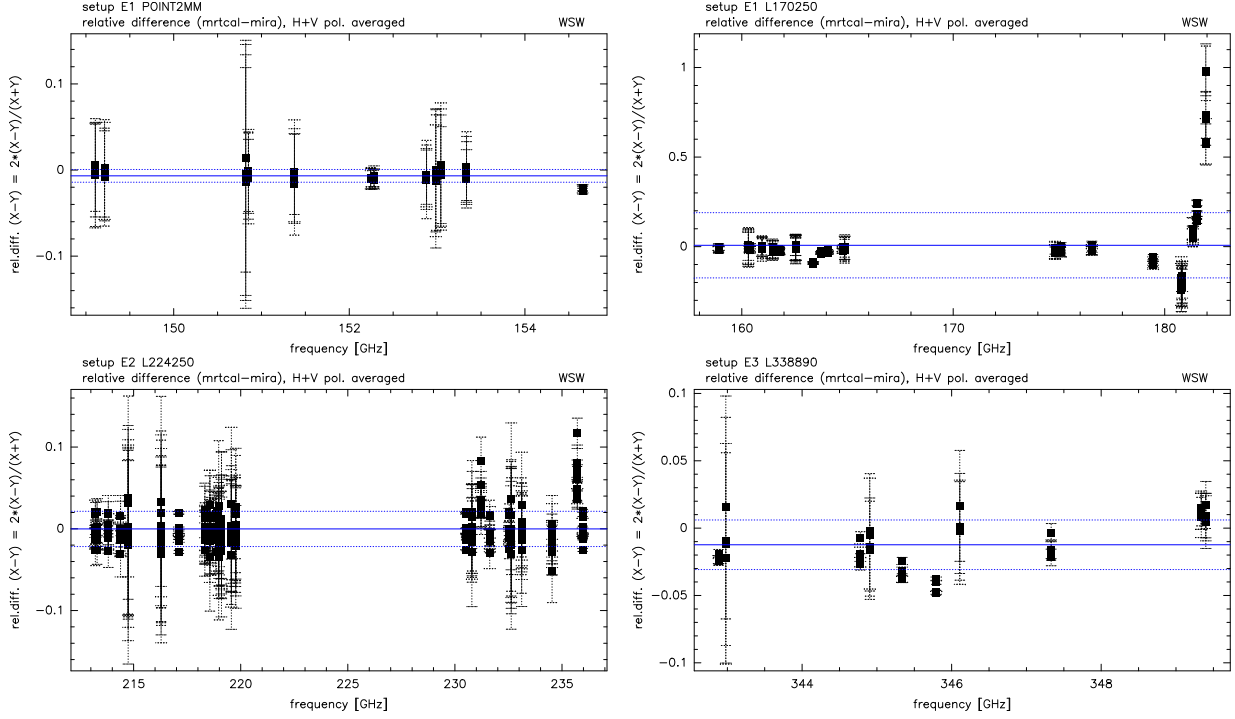


Figure 7: Relative difference of integrated line intensities in **MRTCAL** and **MIRA**-calibrated spectra versus line center frequency for the four frequency setups. One data point is shown per line and scan. Vertical bars indicate the  $3\sigma$  uncertainties estimated from the baseline rms and number of channels in the line. Horizontal blue solid and dotted lines denote the mean value and  $1\sigma$  standard deviation of all points of the respective setup.

mixing with higher order harmonics of the local oscillator frequency. For each selected line, the intensity was integrated over a fixed interval of 29 km/s, equal to the typical linewidth of the source, after subtraction of a baseline of first order in a region of three times the linewidth. The relative difference of integrated line intensities between **MIRA** and **MRTCAL**-calibrated spectra (*i.e.*, the difference of integrated intensities divided by the mean integrated intensity) as a function of frequency is shown in Fig. 7.

The mean of the relative difference over all lines and scans is consistent with zero difference for all frequency setups ( $-0.7 \pm 0.7\%$  for setup E150/POINT2MM,  $1 \pm 18\%$  for setup E150/L170250,  $0.0 \pm 2.2\%$  for setup E230, and  $-1.2 \pm 1.8\%$  for setup E330). This indicates an on-average good agreement of line intensities between **MIRA**- and **MRTCAL**-calibrated spectra. For the E230 setup the maximum relative difference for individual lines is 12%, for the E330 and E150/POINT2MM setup it does not exceed 5%, compatible with the typical expected calibration accuracy<sup>1</sup>. Significant deviations are noted at the high frequency end of the E150/L170250 setup, close to the edge of the 2 mm band atmospheric window, with integrated line intensities in **MRTCAL**-calibrated spectra up to a factor of two higher than those from **MIRA**-calibrated spectra. This particular case will be considered in detail in the following section.





Figure 8: Relative difference of integrated line intensities in **MIRA** and **MRTCAL**-calibrated spectra above 179.4 GHz in setup E150/L170250, at the edge of the 2mm atmospheric window. Top panel: with default 20 MHz calibration bandwidth in **MRTCAL**, which traces better the strong increase of atmosphere opacity at the high frequency end. Bottom panel: with **MRTCAL** calibration bandwidth equal to the natural hardware unit size, i.e. 1.35 GHz for FTS200. Horizontal blue solid and dashed lines indicate the mean and  $1\sigma$  standard deviation of all data points.

## 5 Quantitative impact of the MRTCAL frequency dependent calibration

Opacity increases strongly at the upper end of the EMIR 2 mm band because of the atmospheric water line at 183.3 GHz. Observations near the upper edge of the 2 mm atmospheric band will thus exacerbate

<sup>1</sup>Typical differences of  $5\pm 5\%$  are found between integrated line intensities in horizontal and vertical polarization for all frequency setups. These are not addressed here because they originate from the hardware side, and are consistent between **MIRA**- and **MRTCAL**-calibrated spectra.



Figure 9: System temperature derived by **MIRA** (dashed black horizontal lines, one per 1.35 GHz hardware unit of the FTS200) and **MRTCAL** (dashed blue line) for the upper outer subband of setup E150/L170250. The respective spectra are shown with solid lines.

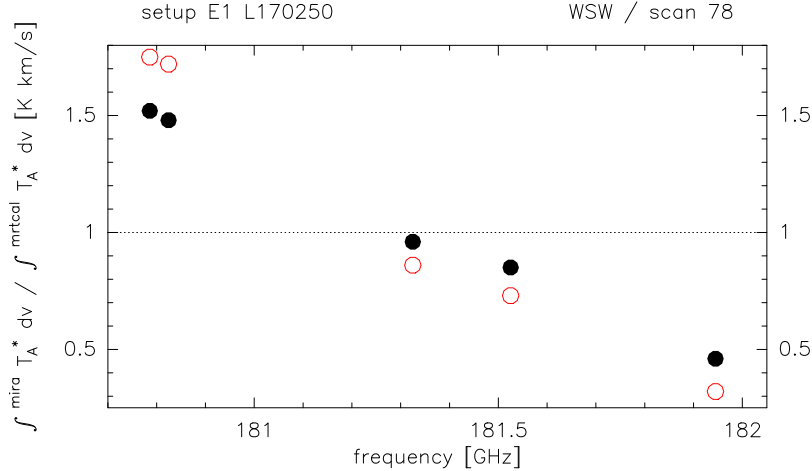


Figure 10: Ratio of integrated line intensities in **MIRA** and **MRTCAL**-calibrated spectra (black) at the upper frequency end of setup E150/L170250, compared with the ratios of system temperature (red) at the line frequencies.

the change in the calibration strategy that should better take into account the frequency dependency.

That the differences in line intensities between **MRTCAL** and **MIRA** close to the atmospheric window are a direct consequence of the different calibration bandwidths, is shown in Fig. 8. The top panel shows the relative difference of integrated line intensities for **MRTCAL** calibration with default settings (*i.e.*, in 20 MHz steps), while the bottom panel shows it for a **MRTCAL** calibration in steps of the natural hardware units, the **MIRA** calibration bandwidth. In the second case, the relative differences are reduced from up to 100% to  $\leq 11\%$ . Residual differences in the bottom panel are possibly due to the remaining difference in the correction of the intermediate frequency bandpass.

The spectra and system temperature derived by both calibration softwares at the edge of the atmospheric window are shown in Fig. 9. In the rightmost third of this figure, the system temperature ( $T_{\text{sys}}$ ) derived by **MRTCAL** better traces the strong increase of atmospheric contribution than the single mean



Figure 11: Integrated intensities of seven lines in the E230 setup for the three switching modes position-switching (PSW, shown as squares), wobbler-switching (WSW; triangles) and frequency-switching (FSW, circles), for calibration with **MIRA** (black) and **MRTCAL** (blue) with default settings. The integrated intensities are normalized to those measured for position switching. Bars indicate the  $1\sigma$  standard deviation over all scans of the according line. The three leftmost lines 1–3 are bright (peak temperature  $T_A^* \sim 6\text{--}10\text{ K}$ ). Lines 4–7 are weaker ( $T_A^* \sim 1\text{ K}$ ).

$T_{\text{sys}}$  value used by **MIRA**. In agreement with this, line peaks in the **MIRA**-calibrated spectrum are underestimated compared to those from **MRTCAL** in the regions where the **MIRA** value of  $T_{\text{sys}}$  is below that of **MRTCAL** (*i.e.*, above 181.2 GHz, see also figure 7), and vice versa. Moreover, the baseline noise at the high frequency end is increased in the **MRTCAL**-calibrated spectrum due to the proportionality to  $T_{\text{sys}}$ , providing a more realistic magnitude in this region of low atmospheric transmission.

Figure 10 shows a numerical comparison of the ratio of the integrated line intensities in **MIRA**- and **MRTCAL**-calibrated spectra with the ratio of the respective system temperature applied at the line frequencies. The ratio of system temperature indeed shows the same trends as the ratio of line integrated intensities. The relative error between the two ratios is of the order of 20%. This could be due either to uncertainties in line intensities or to the scheme used to correct for the bandpass shape that is slightly different between **MIRA** and **MRTCAL**. Additional work is required to explore this discrepancy.

## 6 Comparison of switching modes

All three switching modes available for spectral line observations were observed with the same EMIR 1 mm band setup in order to check the consistency of the line intensities between the different switching mode. To our knowledge, this is the first time this kind of study is done at the 30m-Telescope.

Figures 11 compares the integrated line intensities for seven lines in position, wobbler, and frequency switching mode. In all cases, the individual scans were corrected for the gain-elevation curve as the source is barely resolved. Moreover, both polarizations were averaged. Integrated line intensities from the frequency-switched spectra may suffer from a higher uncertainty due to strong baseline ripples that are associated with this switching mode. This is especially true for the weaker lines.

The integrated line intensities in position-switching are consistent between both calibration software,

with **MRTCAL** intensities reaching  $99\pm1\%$  (mean over the seven lines and its  $1\sigma$  standard deviation) of the **MIRA** intensities.

For wobbler-switching, the integrated line intensities amounts to  $93\pm1\%$  of the intensities in position-switching for both **MIRA**- and **MRTCAL**-calibrated spectra. This reduction of line intensity is expected because of the reduced antenna gain when tilting the subreflector. For a tilt of  $90^\circ$ , the antenna main beam gain at 230 GHz is reduced to 0.93 (see report by Peñalver 2016), in agreement with the observed value.

For frequency-switching, the integrated intensities reach  $94\pm1\%$  of the position-switching intensities for the **MRTCAL**-, and  $89\pm1\%$  for **MIRA**-calibrated spectra. **MRTCAL** delivers integrated intensities that better match the position switching ones, probably because the frequency calibration and folding of the two phases is done in a different way than in the usual combination of **MIRA** and **CLASS**. Indeed, Winkel et al. (2012) indicate that the usual approach underestimates line intensities when the line strengths is not negligible compared to the system temperature.

The remaining difference of  $6\pm1\%$  between frequency-switching and position-switching when the data is calibrated by **MRTCAL** could be related to a lost of receiver efficiency when the frequency throw is large. In our case, it was set to the maximum value of  $\pm 23.4$  MHz because IRC+10216 lines are relatively broad. This effect will be further explored in new observations.

## 7 Calibration stability with time and elevation

Figure 12 shows the integrated line intensity of the strongest lines in the E230 setup as a function of the observation time or the source elevation. The intensities were corrected for the gain-elevation-curve (Peñalver 2012). The correction amounts to about 15% for the lowest elevations of  $25^\circ$ .

The line intensities are relatively stable except between  $44$  and  $54^\circ$  where the intensities appear low compared to the remaining points. This also corresponds to an observing time interval (8.5–9.25 UT) between two pointing observations. An error in the pointing correction could explain this difference.

## 8 Acknowledgments

The authors thank H. Wiesemeyer for useful indications on **MIRA** behavior.

## 9 References

- C. Kramer, 1997 January 24: Calibration of spectral line data at the IRAM 30m radio telescope
- G. Paubert, 2002 August 23: VESPA user's guide.
- J. Peñalver, 2016 April 18: Antenna Gain depending on Wobbler Tilt.
- J. Peñalver, 2012 April 16: Antenna Gain Elevation Curve.
- B. Winkel, A. Kraus, U. Bach, 2012, A&A 540

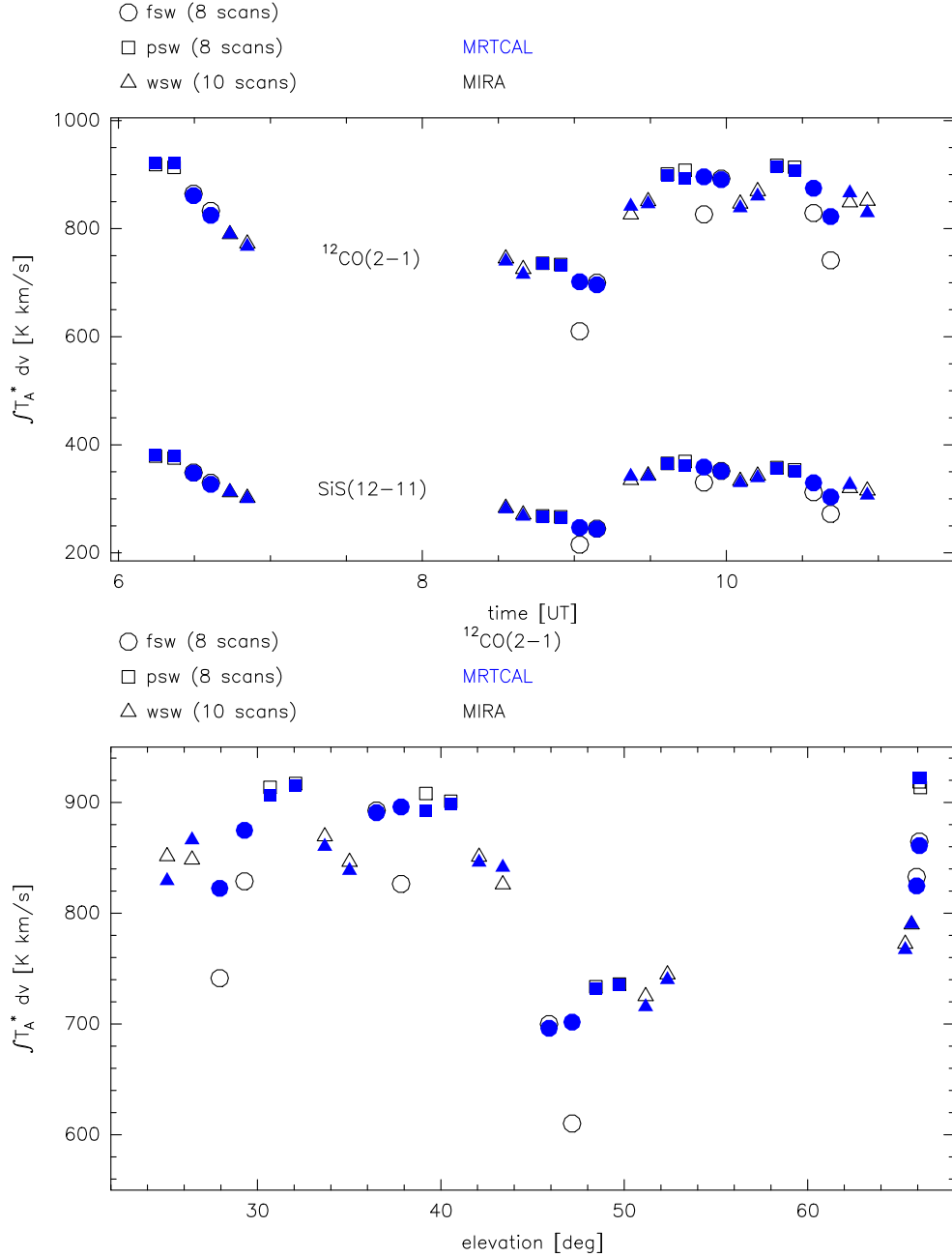


Figure 12: Integrated line intensity in **MIRA** (black) and **MRTCAL** (blue) spectra for the two brightest lines in the E230 setup versus time (top panel), and for the strongest line versus elevation (bottom panel), after correction for the gain-elevation-curve. One data point is shown per scan; the observing sequence consisted of one calibration scan and two science scans of 6 min length.

## A List of used lines

Table 2: List of lines used in the comparison (signal-to-noise-ratio  $> 4$ , not blended).

Setup	Rest frequency [MHz]	Species	Transition	Reference
E150 POINT2MM	149106.9	C <sub>3</sub> H	$^2\Pi_{3/2}$ , J=13/2-11/2 a	C2000
	149212.6	C <sub>3</sub> H	$^2\Pi_{3/2}$ , J=13/2-11/2 b	C2000
	150820.6	C <sub>3</sub> H <sub>2</sub>	$4_{0,4}$ - $3_{1,3}$ Para	C2000
	150851.9	C <sub>3</sub> H <sub>2</sub>	$4_{1,4}$ - $3_{0,3}$ Ortho	C2000
	151375.9	C <sub>4</sub> H	$\nu_7=1$ $^2\Pi_{1/2}$ , J=31/2-29/2 a	C2000
	152243.6	C <sub>4</sub> H	N=16-15 a	C2000
	152282.1	C <sub>4</sub> H	N=16-15 b	C2000
	152879.9	C <sub>4</sub> H	$\nu_7=1$ $^2\Pi_{3/2}$ , J=33/2-31/2 a	C2000
	152986.2	C <sub>4</sub> H	$\nu_7=2$ l=0 $^2\Sigma$ , N=16-15 a	C2000
	153042.4	C <sub>4</sub> H	$\nu_7=2$ l=0 $^2\Sigma$ , N=16-15 b	C2000
	153334.9	C <sub>4</sub> H	$\nu_7=1$ $^2\Pi_{3/2}$ , J=33/2-31/2 b	C2000
	154657.3	HC <sub>3</sub> N	J=17-16	C2000
E150 L170250	158903.0	Si <sup>34</sup> S	J=9-8	C2000
	160312.1	ClAl	J=11-10	C2000
	160375.2	<sup>29</sup> SiS	J=9-8	A2012
	160957.1	C <sub>4</sub> H	$\nu_7=1$ $^2\Pi_{1/2}$ , J=33/2-31/2 a	C2000
	161459.8	C <sub>4</sub> H	$\nu_7=1$ $^2\Pi_{1/2}$ , J=33/2-31/2 b	C2000
	161758.1	C <sub>4</sub> H	N=17-16 a	C2000
	161796.6	C <sub>4</sub> H	N=17-16 b	C2000
	162547.7	C <sub>4</sub> H	$\nu_7=2$ l=0 $^2\Sigma$ , N=17-16 a	C2000
	163376.7	SiS	J=9-8	C2000
	163753.4	HC <sub>3</sub> N	J=18-17	C2000
	164069.1	SiC <sub>2</sub>	$7_{2,6}$ - $6_{2,5}$	C2000
	164770.5	SiC <sub>2</sub>	$7_{6,2}$ - $6_{6,1}$ & $7_{6,1}$ - $6_{6,0}$	C2000
	164868.0	AlF	J=5-4	C2000
	174806.8	C <sub>2</sub> H	N=2-1, J=3/2-3/2	CDMS
	175084.6	<sup>30</sup> SiS	J=10-9	A2012
	176554.7	Si <sup>34</sup> S	J=10-9	A2012
	179446.5	SiC <sub>2</sub>	J=8 <sub>0,8</sub> -7 <sub>0,7</sub>	CDMS
	180786.0	C <sub>4</sub> H	N=19-18, J=39/2-37/2	CDMS
	180824.5	C <sub>4</sub> H	N=19-18, J=37/2-35/2	CDMS
	181324.8	HNC	J=2-1	CDMS
	181525.2	SiS	J=10-9	A2012
	181944.9	HC <sub>3</sub> N	J=20-19	CDMS
E230 L224250	213208.0	SiC <sub>2</sub>	J=9 <sub>4,6</sub> -8 <sub>4,5</sub>	CDMS
	213292.3	SiC <sub>2</sub>	J=9 <sub>4,5</sub> -8 <sub>4,4</sub>	CDMS
	213816.2	<sup>29</sup> SiS	J=12-11	A2012
	214385.7	<sup>29</sup> SiO	J=5-4	A2012
	214741.0	Si <sup>33</sup> S	J=12-11	A2012
	216278.8	c-C <sub>3</sub> H <sub>2</sub>	J <sub>K<sub>a</sub>,K<sub>c</sub></sub> =3 <sub>3,0</sub> -2 <sub>2,1</sub>	T2010
	217104.8	SiO	J=5-4	A2012
	218324.7	HC <sub>3</sub> N	J=24-23	T2010
	218560.5	AlCl	J=15-14	T2010
	218837.0	C <sub>4</sub> H	N,J=23,47/2 - 22,45/2	T2010
	218875.4	C <sub>4</sub> H	N,J=23,45/2 - 22,43/2	T2010

Continued on next page

**Table 2 – continued from previous page**

Setup	Rest frequency [MHz]	Species	Transition	Reference
	218972.8	C <sub>4</sub> H	$\nu_7 = 1^1$ N,J=23,45/2 - 22,43/2, f	T2010
	219099.3	C <sub>4</sub> H	$\nu_7 = 1^1$ N,J=23,47/2 - 22,45/2, e	T2010
	219560.4	C <sup>18</sup> O	J=2-1	T2010
	219767.3	C <sub>4</sub> H	$\nu_7 = 1^1$ N,J=23,47/2 - 22,45/2, f	T2010
	230538.0	CO	J=2-1	T2010
	230793.9	AlF	J=7-6	T2010
	231220.7	<sup>13</sup> CS	J=5-4	T2010
	231626.7	<sup>29</sup> SiS	J=13-12	T2010
	232534.1	SiC <sub>2</sub>	J <sub>K<sub>a</sub>,K<sub>c</sub></sub> =10 <sub>2,9</sub> -9 <sub>2,8</sub>	T2010
	232628.6	Si <sup>33</sup> S	J=13-12	T2010
	232116.3	AlCl	J=16-15	T2010
	234534.0	SiC <sub>2</sub>	J <sub>K<sub>a</sub>,K<sub>c</sub></sub> =10 <sub>8,2</sub> -9 <sub>8,1</sub> & 10 <sub>8,3</sub> -9 <sub>8,2</sub>	T2010
	235713.0	SiC <sub>2</sub>	J <sub>K<sub>a</sub>,K<sub>c</sub></sub> =10 <sub>6,5</sub> -9 <sub>6,4</sub> & 10 <sub>6,4</sub> -9 <sub>6,3</sub>	T2010
	235961.4	SiS	J=13-12	T2010
E330 L3338890	342882.8	CS	J=7-6	A2012
	342980.9	<sup>29</sup> SiO	J=8-7	A2012
	344779.5	SiS	J=19-18	A2012
	344906.0	SiC <sub>2</sub>	16 <sub>0,16</sub> -15 <sub>0,15</sub>	P2011
	345339.8	H <sup>13</sup> CN	J=4-3	P2011
	345795.9	CO	J=3-2	P2011
	346109.9	SiC <sub>2</sub>	14 <sub>2,12</sub> -13 <sub>2,11</sub>	P2011
	347330.6	SiO	J=8-7	A2012
	349337.7	C <sub>2</sub> H	N=4-3, J=9/2-7/2	P2011
	349399.3	C <sub>2</sub> H	N=4-3, J=7/2-5/2	P2011

C2000: Cernicharo, J.; Guélin, M.; Kahane, C., 2000, AASS 142, p.181–215

A2012: Agúndez, M.; Fonfría, J.P.; Cernicharo, J. et al. 2012, A&A 543, 26

T2010: Tenenbaum, E.D.; Dodd, J.L.; Milam, S.N. et al. 2010, ApJS 190, p.348–417

P2011: Patel, N.A.; Young, K.H.; Gottlieb, C.A. et al. 2011, ApJS 193, pp.65

CDMS: Müller, H.S.P.; Thorwirth, S.; Roth, D.A. et al. 2001, A&A 370, L49-L52